



Efficient extraction of high pulse energy from partly quenched highly Er³⁺-doped fiber amplifiers

PABLO G. ROJAS HERNANDEZ,^{1,*} MOHAMMAD BELAL,^{1,2} COLIN BAKER,³ SHANKAR PIDISHETY,¹  YUTONG FENG,¹  E. JOSEPH FRIEBELE,⁴ L. BRANDON SHAW,³ DANIEL RHONEHOUSE,³ JASBINDER SANGHERA,³ AND JOHAN NILSSON¹ 

¹Optoelectronics Research Centre, University of Southampton, Southampton SO17 1BJ, UK

²National Oceanography Centre, European Way, Southampton SO14 3ZH, UK

³Naval Research Laboratory, 4555 Overlook Ave. SW, Washington, DC 20375, USA

⁴KeyW Corporation, 7880 Milestone Pkwy, Hanover, MD 21076, USA

*pgrh1g15@soton.ac.uk

Abstract: We demonstrate efficient pulse-energy extraction from a partly quenched erbium-doped aluminosilicate fiber amplifier. This has a high erbium concentration that allows for short devices with reduced nonlinear distortions but also results in partial quenching and thus significant unsaturable absorption, even though the fiber is still able to amplify. Although the quenching degrades the average-power efficiency, the pulse energy remains high, and our results point to an increasingly promising outcome for short pulses. Furthermore, unlike unquenched fibers, the conversion efficiency improves at low repetition rates, which we attribute to smaller relative energy loss to quenched ions at higher pulse energy. A short (2.6 m) cladding-pumped partly quenched Er-doped fiber with 95-dB/m 1530-nm peak absorption and saturation energy estimated to 85 μ J reached 0.8 mJ of output energy when seeded by 0.2- μ s, 23- μ J pulses. Thus, according to our results, pulses can be amplified to high energy in short highly Er-doped fibers designed to reduce nonlinear distortions at the expense of average-power efficiency.

© 2020 Optical Society of America under the terms of the [OSA Open Access Publishing Agreement](#)

1. Introduction

Erbium-doped fiber amplifiers (EDFAs) and lasers enable versatile and compact optical sources in the wavelength range of ~ 1.5 – 1.6 μ m (e.g., [1–11]), and can readily be cladding-pumped with over 100 W of power from 980-nm diode lasers at low cost. Their wavelength range offers good atmospheric transmission and relative “eye-safety”, highly desirable for LIDAR [2,10,12], remote sensing, and imaging [13]. However, the small cross-sections (absorption as well as emission) of Er³⁺-ions lead to low pump absorption [14–16] and, consequently, nonlinear degradation (e.g., [2,4,7,10,17,18]), which builds up as the signal propagates through the relatively long Er-doped fiber (EDF) (e.g., [2,4,10]) of, say, 10 m. Ytterbium co-doping [19–22] can improve the pump absorption and, to some extent, the gain, in short fibers. Alternatively, a high Er³⁺-concentration can also increase the pump absorption and gain, as well as the energy stored in the excited Er³⁺-ions in a short fiber. However, too high Er³⁺-concentrations lead to harmful quenching [14–16,23–42], which degrades the performance. The resulting impact depends on the amplifier configuration and operating regime [6,33,36,38,41]. Notably, for high-energy pulses, the pulse duration may be shorter than, or comparable to, the quenching time scales, reported to be in the range 50 ns – 10 μ s [36]. By contrast, the quenching process is often assumed to be instantaneous, but this may exaggerate the impact of the quenching on such pulses. Thus, in this regime, a finite quenching time may allow for high-energy pulse amplification at higher quenching-levels than normally considered. Indeed, refined simulations with 2- μ s quenching time showed a modest

pulse-energy penalty of ~10% in an EDFA core-pumped with 10-200 mW at 980 nm [43], but there was no experimental investigation. The fractional unsaturable absorption was not stated, but we evaluate it to 1.7%. This is a quite low level of quenching even compared to commercial low-concentration EDFs [42].

In this paper, we present an experimentally based investigation of the impact of quenching on amplification of high-energy pulses of 6 ns - 20 μ s duration in a cladding-pumped Er-doped fiber with a high Er³⁺-concentration, partly-quenched with 16.3% unsaturable absorption at 1536 nm. Our focus is not on the microscopic details of the quenching, but the effects of the quenching on amplification in this regime. Our key finding is that despite this quenching, it was possible to amplify pulses to high energy in the primarily investigated EDF. Even though the unsaturable absorption was at a level where it severely compromised the power conversion efficiency, the attainable pulse energy was comparable to that expected from an unquenched EDF. Compared to our previous conference publication [44], we now investigate shorter pulses with an improved setup.

2. High-energy pulse amplification in unquenched fiber amplifiers

In the absence of quenching, high-energy pulse amplification in rare-earth-doped fiber amplifiers, including EDFAs, is well understood [1–11,17,45–48]. In the unquenched case, amplified spontaneous emission (ASE) or spurious lasing limits the energy that can be extracted ($E_{extractable}$) in a high-energy signal pulse to a few times the intrinsic saturation energy E_{IS} , or say, at most 10 times [46–48] if the stored energy and the extraction efficiency are both at their practical limits. Specifically, the extractable energy is related to the gain according to [47]

$$E_{extractable} = E_{IS} G_{Np}^{initial}, \quad (1)$$

where $G_{Np}^{initial}$ is the initial gain in nepers when the pulse arrives. The extractable energy (which is a fraction of the energy stored in the EDFA) and thus the gain build up between pulses and generally reach their highest values when the pulse arrives. The small area of a typical core leads to low intrinsic saturation energy, so high-energy amplification in fibers requires high initial gain. However, ASE and spurious lasing limit the gain to at most ~10 Np (or ~43 dB), and thus the extractable energy according to Eq. (1) even in an unquenched amplifier. The extracted energy can be evaluated more precisely with the Frantz-Nodvik equation (FNE) [45], but the limit set by the achievable initial gain remains. Damage and nonlinearities can further limit the pulse energy as well as the peak power (e.g., [7,17]).

3. Concentration quenching

As noted above, EDFs for high-energy pulses are often highly doped to reduce the fiber length and thus the nonlinear degradation, and are therefore likely to suffer from some degree of quenching (often referred to as concentration quenching). Even if the EDF is not fully quenched and is able to reach net gain when pumped sufficiently hard, the quenching still impairs the amplification and may well limit the build-up and extraction of energy. Also quenching has been treated in many publications but there are still considerable uncertainties in the details, and considerable variations between different fibers, even if these are similar in other respects. Generally, non-radiative electric or magnetic multipolar coupling or in extreme cases even so-called direct exchange between neighboring Er³⁺-ions in the metastable upper laser level (⁴I_{13/2}) lead to quenching through energy-transfer upconversion [14–16,23–42]. The strengths of these types of parasitic interactions depend on the distance between the Er³⁺-ions in different ways, and at low concentrations, the separation between Er³⁺-ions can be large enough to make quenching negligible. Tailored host glasses, e.g., co-doped with Al₂O₃ or P₂O₅ [11,14–16,49],

as well as nanoparticle doping [40,41,50–53] can also counteract quenching, but it still reappears gradually at higher concentrations.

Quenching can be understood as a nonradiative lifetime shortening of the upper laser level from the unquenched value of ~ 10 ms. This leads to a distribution of lifetimes depending on the local environment of individual ions, but for simplicity, the ions are often grouped into two classes, clustered ions, which typically exhibit severe lifetime shortening, even to the point where it is difficult to measure, and isolated ions. Whereas also isolated ions can experience some lifetime shortening, e.g., due to so-called uniform or homogeneous upconversion (HUC) involving nonradiative energy-transfer over relatively large distances, the effects are relatively modest [14,15,30,31,34,38,42,49]. Fluorescence decay measurements showed no lifetime shortening when a 25-cm piece of the EDF which is the focus of this paper was cladding-pumped at 980 nm with pulses of 10 μ s duration and 21 W peak power at 12 Hz pulse repetition frequency (PRF). Such excitation is only expected to probe isolated ions. Still, even for those, this leads to no more than around 2% excitation. Furthermore, the detector's response to scattered pump light masked the initial 5 ms of the fluorescence decay. Since lifetime shortening is most pronounced in the initial part of the fluorescence decay and at high Er-excitation levels, we cannot rule out modest lifetime-shortening associated with isolated ions. However, although that could perhaps be significant in the low-power regime, such reduction in lifetime can be fully compensated for by an increase in pump power, and the resulting pump power penalty is less significant at the powers that we used. We rarely used less than 10 W of pump power, and never used all the available pump power. Therefore, we disregard the possible effects of HUC, including the measured modest lifetime-shortening, in this paper.

Instead, the quenching and its impact is often more strongly tied to Er^{3+} -clusters (e.g., pairs) [14–16,31–35,37,38,49]. In those, the nonradiative energy transfer between excited Er^{3+} -ions and the resulting quenching through so-called inhomogeneous upconversion is rapid, orders of magnitude faster than the fluorescence decay of unquenched ions. This makes it difficult or practically impossible to excite more than one ion in a cluster, even if the pump power is increased. Therefore, most of the clustered ions remain in the absorbing ground state, and such a cluster (or pair) forms a quenching center, or a trap. A higher Er^{3+} -concentration increases the fraction of clustered Er^{3+} -ions. It is possible to measure directly the dynamics of the quenching process, by measuring the weak and short-lived fluorescence they emit. Quenching timescales have been reported to lie in the range of 50 ns – 10 μ s [36], and later, by the same authors, restricted to sub-microsecond [38]. However, both the excitation and the detection used in our fluorescence measurements were inadequate for this. We note that other traps such as OH^- are also possible [20], which also make it difficult to excite the Er^{3+} -ions. Even in cases when the relative or even absolute concentration of traps does not depend on the Er^{3+} -concentration, the quenching can still increase at higher Er^{3+} -concentrations due to increased rates of energy migration to traps [20,26–28,54].

Regardless of the details of such rapid quenching, it is often described in terms of a resulting unsaturable absorption [32–35,37,41,42]. Unsaturable-absorption measurements directly probe the fraction of ion that are (strongly) quenched and directly quantify the unsaturable absorption, which we expect is more important for the performance of high-power EDFAs than the much more modest lifetime-shortening characteristic of HUC (e.g., already 10% unsaturable absorption is highly significant, whereas even 50% fluorescence lifetime shortening is negligible in simulations of a representative high-power EDFA). A signal photon emitted inside the EDF may then be lost to unsaturable absorption instead of contributing to the signal output, and an absorbed pump photon may fail to excite an Er^{3+} -ion. A non-zero quenching time means that the saturation characteristics become less distinct, and at sufficiently high probe power density, also the “unsaturable” absorption can saturate, if quenched ions become excited. Similarly, when the fiber is used to amplify pulses of duration shorter than, or comparable to, the quenching timescale,

the pulses may be able to partly saturate the normally unsaturable absorption, if the peak power and energy of the pulses are high enough. In particular, and central to this paper, an ion in the ground state that absorbs a signal photon does not have time to return to the ground state and can therefore not absorb a second signal photon in the same pulse, irrespective of whether the ion is quenched or not. Then, Eq. (1) applies to the ion collective as a whole, and the key question becomes if it is still possible to reach a high initial gain, despite the quenching. As proposed in the introduction, this may reduce the impact of the quenching and allow for high-energy pulse amplification at higher levels of unsaturable absorption than normally considered. We emphasize that the finite quenching time is essential for this hypothesis, whereas other details of the quenching process may be less important.

4. Experimental setup

Our experimental layout is shown in Fig. 1. This comprises an amplified wavelength-tunable pulsed single-mode signal seed source, a pump laser, and dichroic mirrors and lenses for coupling signal and pump light into and out of the Er-doped fiber-under-test (FUT). The pump laser was a pigtailed diode laser (IPG PLD-70-974) with up to 57 W of output power at ~ 975 nm. The launch efficiency was $\sim 85\%$ into the FUT, which had both ends angle-cleaved at $\sim 12^\circ$ to suppress feedback. Counter-pumping from the signal output end was chosen for its higher efficiency in quenched EDFs [6,31,38].

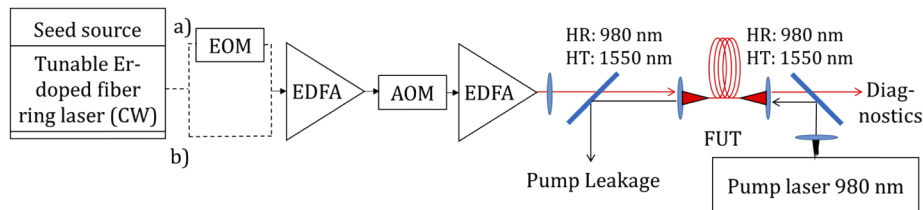


Fig. 1. Amplifier test rig for the FUT. Path (b) is used for signal pulses longer than 50 ns and up to 20 μ s, defined by an acoustic optic modulator (AOM). Path (a) introduces an electro-optic modulator (EOM) to define pulses of 6–50 ns duration. The AOM is then set to 50 ns.

The FUT is fabricated by Naval Research Laboratory (NRL) using MCVD and solution-doping [15,50] and is designated NRL-160415. It has a 0.11-NA, 20- μ m-diameter Er-doped aluminosilicate core centered in a 125- μ m-diameter circular inner cladding, which is coated by a low-index polymer. Figure 2 shows the refractive-index profile of the core together with white-light absorption spectra for the core as well as the pump waveguide (i.e., largely the inner cladding). The core absorption spectrum was measured on a short fiber to avoid errors from saturation and re-emission [55]. It reached 95 dB/m at the 1530-nm peak. Based on preliminary experimental data for different fiber lengths, signal wavelengths, and pulse parameters, we used a signal wavelength of 1560 nm in most amplification experiments, and an optimal length of 2.6 m. The emphasis was on high pulse energy, but this fiber length and wavelength performed well across the range of pulse parameters we used. Thus, the pump-waveguide absorption spectrum in Fig. 2(b) was measured on a 2.6-m long fiber. The circular symmetry of the FUT can lead to poor pump absorption. Therefore, the FUT was coiled to promote mode scrambling and thereby pump absorption [56,57] in one case in Fig. 2(b) as well as in the amplification experiments. The FUT was wound into a triangle-shaped coil around three 2.5-cm-diameter cylinders, 8 cm apart from each other. This improved the white-light absorption in the pump waveguide of the 2.6-m piece from ~ 6.7 to 7.4 dB at the 1530-nm peak. These values can also be compared to the value of $95 \text{ dB/m} \times 2.6 \text{ m} \times (20 \mu\text{m} / 125 \mu\text{m})^2 = 6.3 \text{ dB}$ calculated from the core absorption

and the area ratio. The values are relatively similar. The lower value calculated from the core absorption is unusual. It is possible that this is a result of imperfect overlap (i.e., below unity) of the different modes with the core. We evaluate the V-value to 4.38 at 1560 nm, so the core is expected to support LP-modes 01, 11, 21, and 02. Out of these, the modes with the lowest overlap and thus the highest transmission may dominate the output, leading to a lower measured core-absorption. Note here that even though modes with low overlap with the core are weakly guided and are susceptible to bendloss, the fiber was nearly straight for the core absorption measurements. Alternatively, there are also factors that affect the pump-waveguide absorption measurements. For example, the probe light in the inner cladding may be disproportionately located to the center of the fiber (including the core). One possible reason for this is that the coating absorbs at 1530 nm. As it comes to the absorption at 980 nm, this reaches a peak value of 5.2 dB both with and without coiling. We conclude that the pump absorption is satisfactory, and does not exhibit any significant mode-selective pump depletion effects, which would be detrimental. We calculated a saturation energy of 84.5 μJ from the core area and standard absorption and emission cross-sections at 1560 nm for aluminosilicate EDFs ($1.69 \times 10^{-25} \text{ m}^2$ and $3.04 \times 10^{-25} \text{ m}^2$, respectively). To quantify the quenching, we measured the unsaturable absorption fraction to 16.3% with a probe at 1536 nm with up to 1 W of power, continuous-wave (CW). At longer wavelengths, the saturation power increases, and at shorter wavelengths, the available probe power was smaller. These factors hamper unsaturable-absorption measurements, and 1536 nm was the best compromise. The fiber length was 0.3 m, which gives 20 dB of small signal absorption and allowed for a maximum transmitted probe power of over 400 mW. This is well above the saturation power of unquenched ions of $\sim 3 \text{ mW}$ at 1536 nm, so their absorption is well saturated. For the 16.3% unsaturable absorption at 1536 nm, assuming that this is caused by ion pairs, we calculated the corresponding pair fraction to almost exactly 50% of the ions, whereas the other 50% of the ions would be isolated. The fractional unsaturable absorption with 50% paired ions becomes smaller at longer wavelengths, e.g., 13.3% at 1560 nm. Note that we use standard Er^{3+} :aluminosilicate cross-sections also for the quenched ions for all calculations in this paper, although deviations have been reported [39].

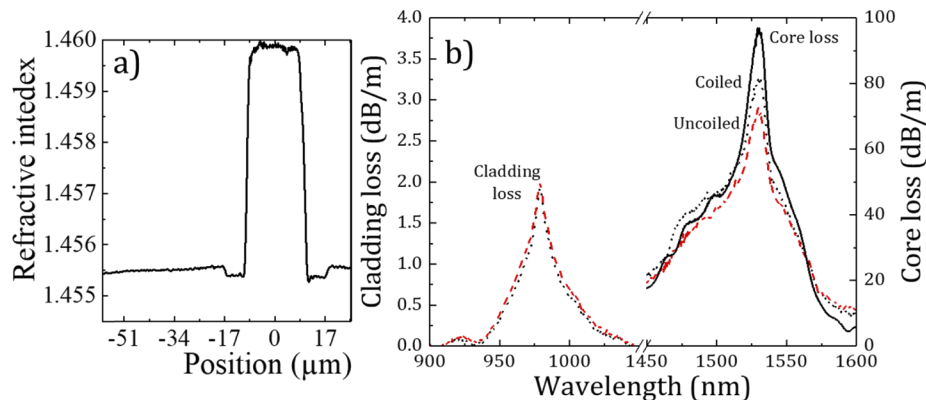


Fig. 2. (a) Refractive index profile and (b) white-light absorption spectra for the FUT (NRL-160415) showing core loss around 1530 nm in a short fiber (black solid curve) as well as pump waveguide (i.e., cladding) loss around 980 nm and 1530 nm for a tightly coiled (black dotted curve) and uncoiled (red dashed curve) 2.6-m-long fiber.

The seed source comprised a tunable CW Er-doped fiber ring-laser with 25 mW of output power, an optional pigtailed electro-optic modulator (EOM, Lucent 2623NA, path *a* in Fig. 1), a pigtailed acousto-optic modulator (AOM, NEOS, shortest time duration 70 ns to reach maximum transmission; 50 ns duration possible with slightly reduced transmission, extinction ratio measured

to 64 dB), and two EDFAs. Optionally, the EOM was by-passed (path *b* in Fig. 1). The pulses produced by the seed source had duration of 6 ns – 20 μ s and energy of 3–60 μ J at 1–40 kHz pulse repetition frequency (PRF). Path *a* was used for pulse durations of 50 ns and shorter, with the EOM running at 12 MHz. The AOM was set to 50 ns duration at the target PRF, to down-sample the pulses and suppress inter-pulse ASE. Path *b* was used for longer pulses, up to 20 μ s in this paper. A dual-channel waveform generator (Tektronix AFG3252) connected to the EOM and the AOM controlled the pulse duration and PRF. The bias of the EOM was regularly adjusted to maintain an extinction ratio (ER) of \sim 20 dB or more.

The first EDFA (IPG EAD-5K-C) in the seed source was operated at constant current for the data we present. It yielded 900 mW of output power with 25 mW of CW-seeding at 1560 nm (path *b*), but lower output power for pulsed seeding (path *a*) with low average input power, e.g., \sim 5 mW with 7.2% duty cycle. Two different EDFAs were used for the second EDFA. In case of path *b*, we used an engineering prototype from SPI Lasers. In case of path *a*, we used an in-house un-packaged EDFA pumped at 1480 nm and based on 3 m of a 5- μ m core EDF from Fibercore (I-15(980/125)HC). Compared to the prototype from SPI Lasers, this was better suited to the low input power to the 2nd EDFA that resulted with path *a*, which could be as low as 10 μ W. For both path *a* and *b*, after all other parameters had been adjusted, the drive current to the second EDFA was set to produce the desired pulse energy. Whereas we focus on the useful signal energy and average power in the pulses, there was also unwanted energy between the pulses from ASE and leakage through the modulators. This includes unwanted inter-pulse energy in the seed, which limited the maximum seed pulse energy. Table 1 lists key characteristics of selected seed pulses. In the pulse energies and average powers we report in this paper, the intra-pulse contributions have been subtracted and are quoted separately. The signal launch efficiency into the core of the FUT was \sim 90%.

Table 1. Characteristics of selected seed pulses at 1560 nm as launched into the FUT and resulting gain and output from the FUT.

Notes (case)	<i>a</i>	<i>b</i>	<i>c</i>	<i>d</i>	<i>e</i>	<i>f</i>
Seed pulse energy	3.5 μ J	3.5 μ J	22.5 μ J	4.5 μ J	1.13 μ J	22.5 μ J
Pulse duration	6 ns	20 μ s	1 μ s	1 μ s	1 μ s	0.2 μ s
PRF	2 kHz	2 kHz	2 kHz	10 kHz	40 kHz	2 kHz
Energy between seed pulses	0.25 μ J	0.05 μ J	1 μ J	0.01 μ J	2.5 nJ	1.5 μ J
Inter-pulse energy fraction in seed	0.067	0.014	0.043	0.0022	0.0022	0.063
Duty cycle	1.2×10^{-5}	0.04	0.002	0.01	0.04	4×10^{-4}
Seed pulse extinction ratio ^g	61 dB	32 dB	40 dB	47 dB	40 dB	46 dB
Path (cf. Figure 1)	Path <i>a</i>	Path <i>b</i>				
FUT output pulse energy	200 μ J	76 μ J	770 μ J	243 μ J	53.7 μ J	800 μ J
FUT output extinction ratio ^g	60 dB	18 dB	29 dB	31 dB	27 dB	36 dB
Resulting energy gain in FUT	17.6 dB	13.4 dB	15.3 dB	17.3 dB	16.8 dB	15.5 dB
Resulting gain for total average power in FUT	17.6 dB	14.7 dB	17.3 dB	17.6 dB	17.0 dB	17.4 dB
FUT pump power	25 W	25 W	50 W	50 W	50 W	50 W

Notes

^aUsed in Fig. 4 (shortest pulse duration), and in Fig. 5.

^bUsed in Fig. 4 (longest pulse duration).

^cUsed in Fig. 6 (point with highest output energy).

^dUsed in Fig. 6 (point with highest average signal output power).

^eUsed in Fig. 6 (point with highest PRF).

^fUsed in Fig. 7 (point with highest output energy), and in Figs. 8 and 9.

^gRatio of average instantaneous power (energy/duration) in a pulse to that between pulses.

Diagnostics include an optical spectrum analyzer (OSA, ANDO AQ6317B). This was used in CW measurement mode with sufficiently low measurement bandwidth to measure the time-averaged spectrum. For temporal measurements, we used a 1-GHz oscilloscope with 12 bits of vertical resolution (Agilent DSO9104H) and InGaAs photodetectors (Thorlabs DET10C, 35 MHz, detector area 0.8 mm^2 , bias voltage 5 V, and EOT ET-3500, $\sim 15 \text{ GHz}$, area $8 \times 10^{-4} \text{ mm}^2$). Since the leakage through the modulators in the seed occurs largely at the seed wavelength, we determined the pulse energy from the average power and oscilloscope traces and checked there were no inconsistencies in the optical spectrum (e.g., excessive ASE). See Appendix for details. Average optical powers were measured with thermal and semiconductor power meters.

5. Continuous-wave characteristics

Figure 3 shows the gain for a CW seed with 1 mW of launched power at 1560 nm. This reaches $34 \text{ dB} = 7.8 \text{ Np}$. The pump leakage was $\sim 30\%$ (-5.2 dB) at high gain. Thus, the pump absorption is similar to the white-light absorption at the 980-nm peak, despite the significant excitation of Er^{3+} -ions, and any non-ideal spectral overlap between the pump and the absorption. A possible explanation is that the spatial overlap with the Er^{3+} -ions is larger for the pump light than for the white light used in Fig. 2. The gain slope in Fig. 3 drops at high pump power due to gain saturation, as the signal output power exceeds 2 W. Lower seed power reduces the saturation, but 1 mW is reasonably representative of the seed's parasitic inter-pulse power, so the measured gain is an indication of what initial gain may be achievable (i.e., $G_{Np}^{initial}$ in Eq. (1)). Note however that during high-energy pulse amplification, the instantaneous gain varies continuously in time, and the precise initial gain was not measured in the pulsed experiments. The differential conversion efficiency from pump to signal power in the saturated regime becomes 12% with respect to absorbed pump power for the data in Fig. 3. In simulations with 50% of paired ions and the signal gain deeply saturated, the signal output power increases linearly with the pump power with a slope (i.e., differential conversion efficiency) of 18%. Here, the quenching of pairs was assumed to be instantaneous, since it is expected to be much faster than Er^{3+} absorption and stimulated-emission rates in the CW case. For example, in Fig. 3, typical transition rates correspond to a time scale of, e.g., 0.1 ms. Without quenching, the simulated differential conversion efficiency was at the quantum limit of 63%, which is $\sim 7 \text{ dB}$ higher than the experimental value, and 5.5 dB higher than the simulations with 50% of the Er-ions in pairs. This underlines the strong detrimental impact of quenching in the CW regime. Nevertheless, the high gain that we reach may allow for high pulse energies, according to Eq. (1).

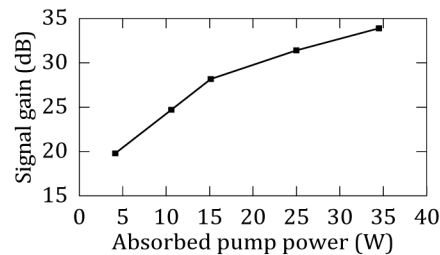


Fig. 3. Gain vs. absorbed pump power for 1 mW of CW input signal at 1560 nm.

6. Pulse amplification results and discussion

Figure 4 shows the output signal pulse and inter-pulse energy vs. pulse duration for 2-kHz PRF, 3.5- μJ seed energy (average seed power 7 mW), and 25 W of launched pump power (17 W absorbed). The pulse duration varies from 6 ns to 20 μs , and the seed's peak power from ~ 580

W down to ~ 0.17 W. The EOM (path *a*) is used only for durations of 50 ns and less. The total output power as measured with a thermal power meter is also shown, in terms of the total energy during the pulse period, i.e., the average power divided by the PRF. For the longest pulses (20 μ s), the output energy reaches 68 μ J, so the energy gain becomes 13 dB. The total average output power becomes 190 mW. The ER becomes 18 dB in terms of the power during the pulses relative to the average power between pulses. The stimulated-emission rates induced by the input and output signal pulses become ~ 1290 $s^{-1} = (770$ μ s) $^{-1}$ and $\sim 25,100$ $s^{-1} = (40$ μ s) $^{-1}$, respectively, if we assume that the pulses are rectangular. All these values then increase for shorter pulses. Thus, for 6-ns pulses, the energy gain increases by 5 dB from that of the 20- μ s pulses and reaches 18 dB. The ER becomes 60 dB, and the total average output power becomes 450 mW. The output pulse energy reaches 0.2 mJ energy (~ 2.4 times the saturation energy). For comparison, the FNE yields 0.27 mJ of output pulse energy with standard cross-sections for an unquenched EDF and 28 dB of initial gain, obtained from Fig. 3 for 17 W of absorbed pump power. This is only 1.5 dB higher than the experimental result for 6-ns pulses. The stimulated-emission rates induced by the input and output signal pulses become $\sim 4.3 \times 10^6$ $s^{-1} = (230$ ns) $^{-1}$ and $\sim 250 \times 10^6$ $s^{-1} = (4.1$ ns) $^{-1}$, respectively, if we assume that the pulses are rectangular. This is comparable to, or faster than, reported quenching rates [36,38].

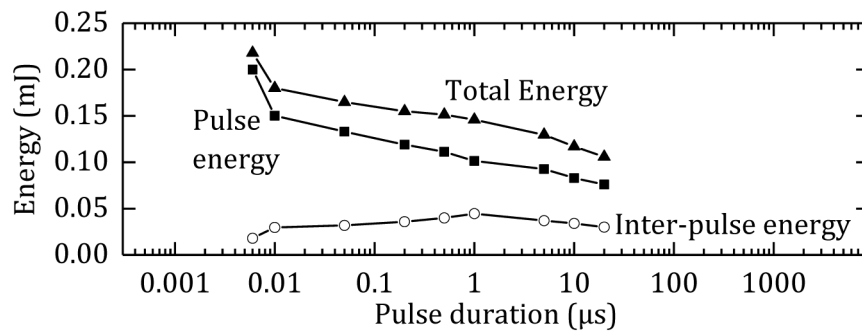


Fig. 4. Output pulse, inter-pulse, and total energy vs. pulse duration for seed energy of ~ 3.5 μ J, PRF of 2 kHz, and launched pump power of 25 W (17 W absorbed).

Figure 5(a) shows the temporal input and output profile of the 6-ns pulse that produced the highest energy of 0.2 mJ in Fig. 4. The output reaches 40 kW of peak power. Figure 5(b) shows the average-power spectrum. With 40 kW of peak power, the nonlinear effect of four-wave mixing generates sidebands (e.g., [7,17,18]) containing $\sim 44\%$ of the energy. Sideband energy is included in all reported energies, but is negligible in most cases.

When we take into account the uncertainties resulting from possible differences between quenched and unquenched erbium cross-sections [39,43] and in other experimental parameters, as well as the spectral broadening, Fig. 4 suggests that for sufficiently short pulses, it is possible to recover the energy gain of unquenched fibers, as described by the FNE, also in our quenched fiber. This is a key result of our experiments. As outlined briefly above, we propose the following explanation: The dynamics of Er^{3+} -ions may be slow compared to the pulse duration. Then, all transitions during the pulse are negligible, compared to those induced by the high-energy signal pulse. This applies to unquenched as well as quenched ions, insofar as the quenching dynamics are slower than the pulse duration. Thus, even if the absorption of quenched ions (in the ground state) is effectively unsaturable in the CW regime, it behaves as a saturable absorber with a short pulse, just like unquenched ions in the ground state do. If other differences in the spectroscopy of quenched and unquenched ions are small, it no longer matters to the pulse if the ions in the absorbing ground state are quenched. Partly quenched and unquenched fibers should then yield similar output pulse energy for the same initial gain. By contrast, for longer

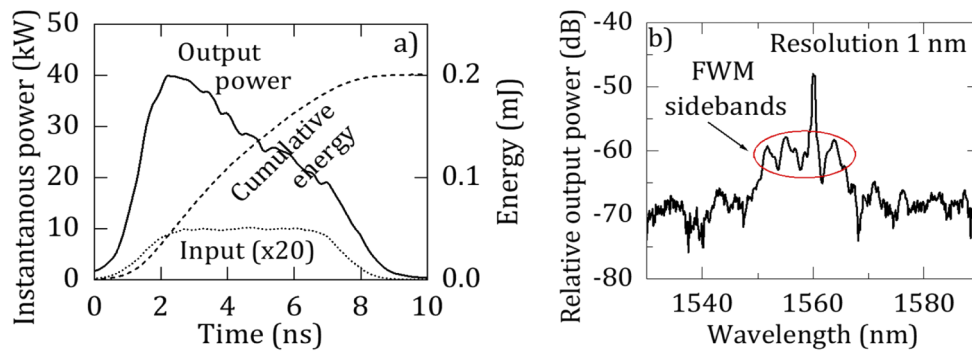


Fig. 5. (a) Instantaneous signal input power (x 20) and output power and cumulative output pulse energy from the beginning of the pulse and (b) optical spectrum for 6-ns pulse duration at 17 W of absorbed pump power. Case (a) in Table 1.

pulses, a quenched ion that absorbs a signal photon has time to lose its energy through parasitic nonradiative processes during the pulse and return to the ground state. It can then absorb another signal photon in the same pulse, leading to lower output energy. Thus, the measured output energy recovers its unquenched value for shorter pulses in Fig. 4, but decreases significantly for longer pulses. Such dependence is not expected for unquenched fibers. We hypothesize that it also helps to maintain the ER for shorter pulses, but not for longer pulses (cf. Table 1), although further investigations would be needed to confirm that.

Although Fig. 4 shows higher output energy for shorter pulses, this was with pulse seed energy limited to $\sim 3.5 \mu\text{J}$ and with non-negligible inter-pulse seeding. Therefore, for the seeding used in Fig. 4, higher pump power than 17 W (absorbed) rapidly increased the energy between the pulses rather than in the pulses. Higher seed energy may lead to higher output energy, although this was beyond the capability of our seed source for the 6-ns case in Figs. 4 and 5. With longer pulses, however, the seed source can reach higher pulse energy with acceptable inter-pulse energy and power, thanks to the lower gain of the amplifiers. Thus, the FUT can be pumped with higher power and reach higher initial gain, which opens up for higher output pulse energy. Figure 6(a) depicts the average output power and pulse energy vs. PRF for a constant average seed power of 45 mW in 1- μs seed pulses at three wavelengths, 1555 nm, 1560 nm and 1565 nm, with 50 W of launched pump power (35 W absorbed). The PRF varied from 1 to 40 kHz, so the corresponding seed energy varied from 45 μJ down to 1.1 μJ . The results across the three wavelengths show a ~ 6 dB increase in average output power for an increase in PRF from 1 kHz to 10 kHz. This is expected, because of decreasing energy saturation and inter-pulse ASE for higher PRF. For an unquenched system, one expects this trend to continue with a further increase in average output power also for PRF above 10 kHz, asymptotically towards a maximum for high PRF. Instead, Fig. 6(a) shows a small drop in power. We propose this is another, more subtle, result of quenching. Even if a short pulse saturates the absorption of the quenched ions by exciting them for the duration of the pulse, the energy in the excited quenched ions is then rapidly dissipated through the quenching process. The saturation implies that the absorbed energy increases sub-linearly with pulse energy, so lower-energy pulses at higher PRF increase the fraction of the pulse energy, and thus the average power, deposited into the quenched ions. This reduces the average output power for higher PRF.

The decrease in power for higher PRF is confirmed in Fig. 6(b), which shows the total output power as measured with a thermal power meter. It also shows the average inter-pulse power. In conventional fashion, the inter-pulse power is high at low PRF and lower for higher PRF. The inter-pulse power at 1555 nm and 1565 nm is significantly higher than at 1560 nm, especially at high PRF. This leads to an unusually strong wavelength dependence in Fig. 6(a). For PRF lower

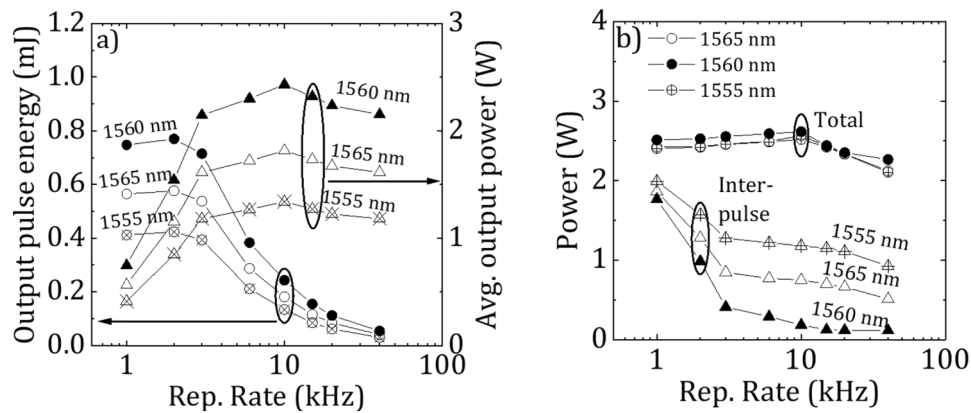


Fig. 6. (a) Output pulse energy and average signal power vs. PRF at constant average signal input power of 45 mW in 1- μ s pulses at three wavelengths, 1555 nm, 1560 nm and 1565 nm with 50 W of launched pump power (35 W absorbed). (b) Total output power (combined in pulses and between pulses) and inter-pulse power.

than 3 kHz, the rapid increase in inter-pulse power hampers further pulse-energy growth, and the inter-pulse power reaches over 45% of the average signal power already at 2 kHz. Although ASE is generally bi-directional, the FUT is seeded in the forward direction by inter-pulse power from the seed laser (ASE as well as leaked signal). Compared to the forward inter-pulse energy, we expect backward-propagating inter-pulse power to be negligible.

We next consider the effect of pulse duration in this regime of high-energy seeding and extraction. For this, the parameters are the same as in Fig. 6, except that we seed at 1560 nm and vary the pulse duration from 0.2 μ s to 10 μ s with PRF in the range 1 to 10 kHz. The duty cycle varies between 2×10^{-4} (0.2 μ s, 1 kHz) and 0.1 (10 μ s, 10 kHz). The seed energy varies between 4.5 μ J at 10 kHz and 45 μ J at 1 kHz. The average power during the seed pulses varies between 0.45 W and 225 W (this is similar to the peak power of the seed pulses, but at high seed energy, saturation-induced pulse shortening can be significant already in the seed). The results are shown in Fig. 7. We see that the trend with respect to PRF is the same as in Fig. 6. Furthermore, the trend with respect to pulse duration is the same as in Fig. 4, (i.e., the shortest pulse of 0.2 μ s leads to the highest energy, which is reached at 2 kHz rather than at 1 kHz, although the difference in output energy may be too small to be significant. Thus, with 2-kHz PRF seeding in 0.2- μ s pulses (so with 22.5 μ J energy and 110 W average power and $\sim 0.84 \times 10^6$ $s^{-1} = (1.2 \mu s)^{-1}$ stimulated-emission rate during the seed pulse), the maximum pulse energy from the FUT reaches as high as 0.8 mJ, despite a conversion of no more than 4.6% of absorbed pump power. Figure 8 shows the corresponding input and output instantaneous power and cumulative pulse energy, and Fig. 9 shows the spectrum of the output pulses. The FWHM duration becomes 110 ns, and the actual peak power 6.2 kW, leading to a stimulated-emission rate of $\sim 47 \times 10^6$ $s^{-1} = (21 \text{ ns})^{-1}$. The energy between pulses becomes 53 μ J and the ER 36 dB. The spectral purity is relatively good, with 89% of the power at the signal wavelength. The energy gain reaches 15.5 dB. The energy of 0.8 mJ is 9.5 times the estimated saturation energy, and is 1.5 dB higher than the 0.57 mJ calculated with the FNE, with initial gain of 34 dB (estimated from Fig. 3) and seed energy of 22.5 μ J. Thus, as for the 6-ns pulse in Fig. 5, the agreement with the FNE is fair, but in contrast to the 6-ns pulse, the energy is now higher than that predicted by the FNE. Possible contributions to this difference include energy measurement errors, errors in the estimate for the initial gain used in the FNE, the increased ability of a higher-energy seed pulse to extract energy also in the edges of the core where the signal intensity is relatively low as well as from

any Er^{3+} -ions with atypically small cross-sections, and the increased ability of a higher-power pump to excite paired Er^{3+} -ions, which may have smaller cross-sections [39,43] and thus store more energy for a given contribution to the gain. We also note that measurements with the same seed energy and PRF on a low-quenched EDF (unsaturable absorption 4.5% at 1536 nm) agreed well with the FNE. This EDF was also fabricated by NRL but with nanoparticle-doping [53] and a lower Er-concentration (peak core absorption 33 dB/m) to avoid quenching.

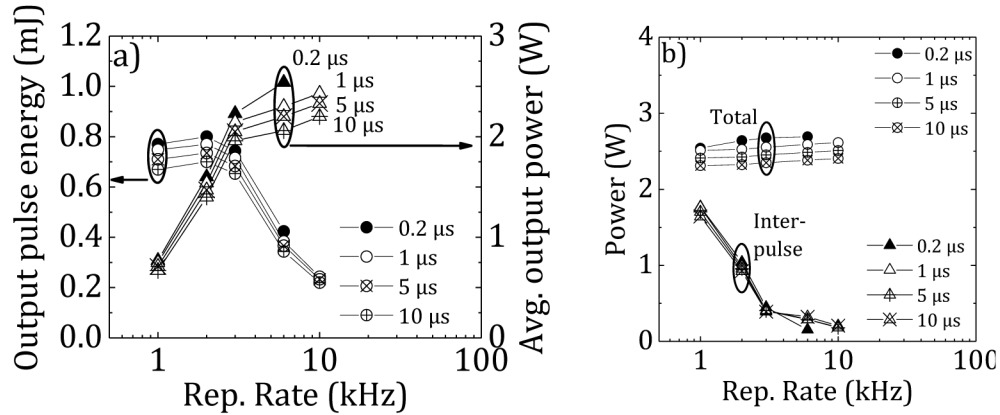


Fig. 7. (a) Output pulse energy and average signal power vs. PRF at constant average signal input power of 45 mW at 1560 nm for different pulse durations with 50 W of launched pump power (35 W absorbed). (b) Total output power (in pulses plus between pulses) and inter-pulse power.

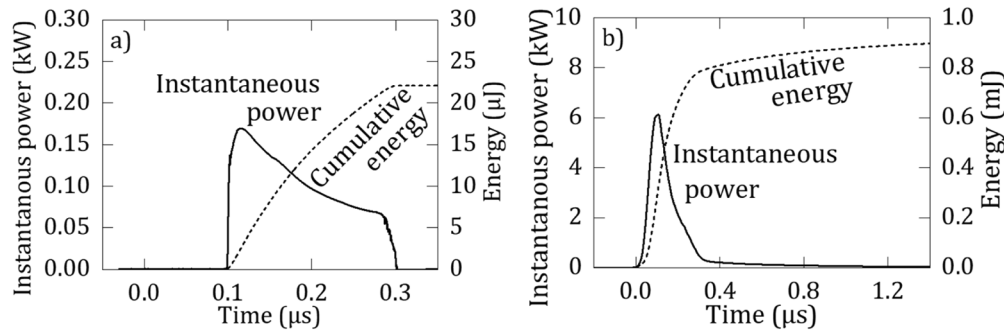


Fig. 8. Instantaneous power and cumulative energy for highest achieved energy (case (f) in Table 1) for (a) input pulses and (b) output pulses.

Even if the effect of the quenching on the extraction process is small and the pulse energy is well described by the FNE, it is possible that the erbium excitation reached in the pumping process, and thus the initial gain, is more strongly affected by quenching. Based on the CW signal gain of 34 dB at 1560 nm for 35 W of absorbed pump power, we roughly estimate that 55% of the Er^{3+} -ions are excited when a pulse arrives. This is a relatively low percentage, which may partly be a result of quenching-induced degradation of the pumping process. Under the assumption of equal spectroscopic parameters for isolated and paired ions, we estimate that 40% of the paired ions and 70% of the isolated ions are excited, as averaged over the fiber, when a pulse arrives. Still, even if the pumping is degraded, the 2.6-m long partly-quenched EDF outperforms unquenched silica EDFs (e.g., [1,4]) in generation of energy per unit core area and length ($0.98 \mu\text{J}/\mu\text{m}^2/\text{m}$) and gain per unit length ($>5.9 \text{ dB/m}$) at 1560 nm. Although the conversion efficiency

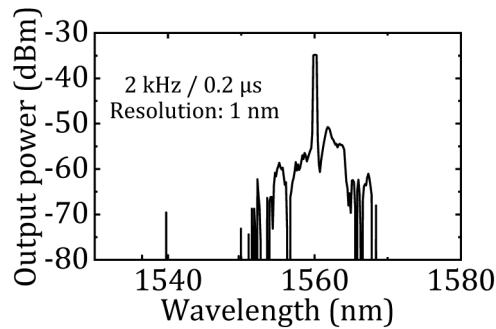


Fig. 9. Output spectrum. Case (f) in Table 1.

decreases, our results show that readily available pump power is more than enough to make the pulse energy limited by radiative losses to parasitic inter-pulse emission (including ASE) rather than by nonradiative quenching losses.

7. Influence of composition, cluster size, and pump direction

It is interesting to compare our results to those reported from EDFs with lower quenching. We note first that similar Er^{3+} -concentrations as in our partly-quenched EDFs are possible with less quenching, as demonstrated with a $\text{P}_2\text{O}_5:\text{Al}_2\text{O}_3:\text{SiO}_2$ glass matrix [11] (we estimate the fraction of unsaturable absorption to be half of that in our fiber). This allowed for pulse amplification with relatively high efficiency (8.4%) in a 1.7-m long EDF with a 35- μm core to 84 kW in 2-ns pulses [11] (energy extraction $\sim 0.1 \mu\text{J}/\mu\text{m}^2/\text{m}$). Thus, it is clear that the relation between Er^{3+} -concentration, quenching, and unsaturable absorption is not unique. We also investigated a second partly-quenched EDF. Those investigations showed that the relation between the unsaturable absorption and the impact on high-energy pulse amplification is not unique, either. Although it had a lower fraction of unsaturable absorption (12% at 1536 nm) than the first partly-quenched EDF presented in this paper, we could not extract high pulse energy. It is possible that it suffers from exceedingly fast quenching by direct exchange [23,24]. This was an experimental nanoparticle-doped aluminosilicate EDF [53]. Nanoparticle-doping can reduce the quenching, but we selected this EDF for its unusually high quenching, and it is possible that also the quenching characteristics differ from those in EDFs fabricated in other ways. A hypothesis is that when the fabrication of a NP-doped fiber preform is unsuccessful, it leads to pairs or perhaps larger clusters of Er^{3+} -ions with very small separation and thus to fast quenching. Note here that for paired ions, according to the model of quenching, it is possible to excite half of the ions even if the quenching process occurs instantaneously (when both ions become excited). It is therefore possible to reach gain also in such paired ions for wavelengths longer than the zero-phonon wavelength of 1530 nm. At 1560 nm, this requires a 0.98- μm pump intensity of $0.13 \text{ mW}/\mu\text{m}^2$, to excite 36% of the paired ions, under the assumption of standard cross-sections and unquenched lifetime, and instantaneous quenching. This intensity translates to as little as 1.5 W of pump power in our fiber. Higher pump power as well as a non-zero quenching time are expected to increase the gain from paired ions, whereas larger clusters would be expected to exhibit less gain (if any), under the assumption that only one ion per cluster can be excited. This suggests that EDFs that do not show any gain are quenched by larger clusters or other defects or impurities such as OH. Detailed spectroscopic studies beyond the scope of this work are needed to evaluate such factors and the impact on high-energy pulse amplification.

Finally, we mention that at low repetition rates, the gain that can be reached during the buildup phase between pulses is independent of the pump direction, if the inter-pulse leakage from the seed source and feedback from the fiber ends are negligible. Furthermore, insofar as the FNE is accurate, the energy extraction depends on the total gain, but not on its distribution. Thus, it may be possible to achieve similar pulse energy with co-directional pumping as we have reached with counter-pumping. However, more energy is normally extracted from the output end of the fiber than from the input end. Co-pumping then requires the pump light to travel further through the partly quenched EDF to replenish the energy, and is therefore likely to be less efficient (i.e., the stored energy will recover more slowly at a given pump power).

8. Conclusions

In summary, our results demonstrate that short pulses can efficiently extract high energy from a partly-quenched high-concentration erbium-doped fiber amplifier, even though the fiber exhibits significant unsaturable absorption in the CW regime. We reached up to 0.8 mJ of output energy from a short (2.6 m) EDFA, which is 9.5 times the estimated saturation energy. Although such results have not been reported before as far as we are aware, the high energy extraction in a short pulse can be readily understood in terms of the dynamics of the quenching process. Thus, we attribute the high energy achievable in this regime to the rapid extraction of stored energy, on time scales faster than the quenching dynamics. Thereby, the short high-energy pulses can saturate the absorption of ions which are unsaturable in the CW regime. This implies that insofar as it is possible to reach a high small-signal gain, it is possible to generate pulse energies of several times the saturation energy. We reached output energies within 1.5 dB of those predicted by the Frantz-Nodvik equation for the unquenched case. Furthermore, in some pulse regimes, the average-power conversion efficiency increased in ways that would not be expected for an unquenched EDF. On the other hand, the impact of the quenching on the average-power conversion efficiency was large, and led to a 7-dB degradation in the CW regime. Furthermore, the amplification of high-energy pulses was severely compromised in another EDF with partial quenching, and we hypothesize that the quenching timescale may be much faster in that fiber. Further studies of the details of different quenching and parasitic processes (which may involve higher-lying energy levels [42]) in different regimes are needed to better understand the impact on high-energy amplification, and how it may depend on composition and fabrication details. Particularly interesting is to what extent the positive results of high-energy pulse amplification in partly-quenched EDFs reported here carry over to hosts and fabrication approaches known for low quenching, at even higher Er-concentration where significant quenching reappears also in such hosts.

Appendix A: Determination of pulse energy from oscilloscope traces

We measured temporal traces at different bandwidths with biased photodiodes and a digital storage oscilloscope (Agilent DSO9104H) to determine the shape, duration, and energy of our pulses. The shape and duration are provided directly by such measurements. For that, a dynamic range of 20 dB and a bandwidth of 1 GHz are typically adequate and easily obtainable. We measured pulse shapes with the 15-GHz detector (EOT ET-3500) connected directly to the oscilloscope with 50- Ω termination and 1-GHz bandwidth.

If the average power is measured separately, it is in principle straightforward to calibrate the oscilloscope trace in terms of instantaneous power and then from that also determine the peak power. The relation to the pulse energy is then a straightforward integration. However, although conceptually simple, this calibration is often challenging, especially at low PRF, where the long interval between pulses can lead to significant inter-pulse energy even at low inter-pulse power in the form of ASE and / or leaked signal. Inter-pulse power is a common issue with high-energy fiber sources, because of the high initial gain they reach. This is a problem for the assessment

of pulse energy as the average power divided by the PRF, which fails to exclude the energy between pulses, as well as through the integration of the pulse trace, because the low duty cycle means that the inter-pulse signal needs to be measured accurately even when it is a very small fraction of the peak power. Consequently, given the level of sensitivity and accuracy required to determine the pulse-energy at low duty cycle, it is sometimes even claimed that the ASE power cannot be detected by a standard photodetector [9]. To overcome this problem, an AOM can be used as a time-gate [8] to separately measure the average power during and between pulses. Alternatively, instead of numerical integration of the digitized oscilloscope trace in a computer, one can integrate the photodetector signal in an analog electronic circuit [9]. This has been found to work well for 100-ns pulses at 10-kHz PRF with a bespoke circuit, although at a relatively small dynamic range (on-off ratio) of ~ 30 dB [9].

In our case, we determined the pulse peak power to be as high as 60 dB above the inter-pulse power for the 0.2-mJ, 6-ns pulse in Fig. 5(a) (case (a) in Table 1). This is much more than the dynamic range of oscilloscopes. In order to determine the pulse energy with such high on-off ratios, we used the large-area detector (Thorlabs DET10C) and reduced the bandwidth with a low-pass circuit comprising a 4.7 nF capacitor in parallel with a 150- Ω resistance, 50 Ω of which was in the oscilloscope's input port. This results in a bandwidth calculated to ~ 226 kHz, which agrees well with the filter's measured time constant T_{LP} of ~ 682 ns. Note that for a pulse significantly shorter than the filter's time constant, the peak signal voltage is given by the charge generated by the pulse divided by the capacitance, and is therefore proportional to the pulse energy. On the other hand, although the peak current through the oscilloscope is reduced as the capacitor is charged and discharged, the full charge will still pass through the oscilloscope. Thus, the integral of the trace over the pulse remains the same. Still, even with this reduction, the 0.2-mJ, 6-ns pulse in Fig. 5(a), would generate a voltage as high as $0.2 \text{ mC} / 4.7 \text{ nF} = 42.5 \text{ kV}$, if we assume a detector responsivity of $1 \text{ A/W} = 1 \text{ C/J}$. We therefore attenuated the light incident on the detector to yield a peak voltage V_{pulse} of up to around 0.3 V over the oscilloscope's 50 Ω (and another 0.6 V over the 100- Ω resistor in series), so by ~ 46.7 dB for the pulse in Fig. 5(a). (Since the voltage is proportional to the optical power or energy, we use a multiplier of 10 in the dB scale rather than 20, as normally used for voltages.) We attenuated the light reaching the detector by passing it through a multimode patchcord, which collected a small fraction of the output signal. For this, the signal was first passed through a diffuser, so that the collected light is representative of the whole beam. The use of a patchcord also shields the detector from ambient light.

We next consider how the inter-pulse power affects the determination of the pulse energy. Relative to the pulse energy E_P , the inter-pulse energy E_{IP} is given by $(V_{IP}/V_{pulse})(T/T_{LP} - 1) \approx (V_{IP}/V_{pulse})(T/T_{LP})$, where T is the pulse period and V_{IP} is the average value of the inter-pulse voltage. For a PRF of 2 kHz, $T/T_{LP} = 733$ (28.7 dB). It follows that V_{IP} needs to be measured with an accuracy of around 40 dB relative to V_{pulse} in order to determine the pulse energy to within 10%. This translates to 30 μV in case of a peak oscilloscope voltage of 0.3 V. At the 50-mV/div oscilloscope gain used in this case, the noise level is specified to 641 μV , and the resolution becomes 488 μV with 12-bit digitization. Although these values are in themselves inadequate, we reduced the inter-pulse error through integration (which is equivalent to averaging). With $T = 0.5$ ms and an oscilloscope setting of 10 MSa/s, there are nearly 5000 samples between pulses, which is expected to reduce the average noise contribution from each sample to the integrated value to $641 \mu\text{V}/5000^{1/2} = 9.1 \mu\text{V}$. Although this is expected to be sufficient, we in addition ensemble-averaged over 256 traces in the oscilloscope. This results in cleaner traces with an expected noise level in each sample of $641 \mu\text{V}/256^{1/2} = 40 \mu\text{V}$. This averaging also improved the resolution of the oscilloscope to 33 μV through internal data processing. The expected noise averaged over 5000 points becomes 0.67 μV , which is well over an order of magnitude better than needed.

It is clear from above that random errors (noise) can be reduced to sufficiently low levels by averaging and integration, but we must also consider systematic errors. One source is the non-zero reading present in the absence of light (the dark-level). We measured this immediately after the pulses with the same oscilloscope settings and averaging and subtracted it from the pulse traces. At 50 mV/div, the dark-level was $\sim 300 \mu\text{V}$. When measured several times within a few minutes, the averaged value varied in a range of around $35 \mu\text{V}$. At 1 mV/div, the dark level was $\sim 100 \mu\text{V}$ and varied over a range of around $8 \mu\text{V}$. These values are large compared to the $1.25 \mu\text{V}$ corresponding to the specified dark-current of the detector of 25 nA or less. Furthermore, the different dark-level characteristics for different oscilloscope settings show that at least some of the characteristics depend on the oscilloscope and are not intrinsic to the detector.

Quantization is also a potential source of systematic errors. A dark-trace that is highly stable with negligible noise leads to a quantization error that is nearly the same in each sample and will not be reduced by integration. This is true also for integration of a mostly-constant inter-pulse trace. In case of $33 \mu\text{V}$ resolution in the quantization, this can lead to a systematic error in the range of $\pm 16.5 \mu\text{V}$ in both the inter-pulse trace and the dark trace. However, in the presence of noise or controlled variations with appropriate distribution, the quantization error becomes random with zero mean and can be reduced by averaging [58,59]. In case of Gaussian noise, a standard deviation of 0.7 or more, relative to the quantization resolution, makes this possible. According to simulations, at that level of Gaussian noise, averaging over 10^8 samples brings the residual quantization error to 40 dB below the quantization resolution, as expected for random errors. Although we had a much smaller number of inter-pulse samples, 5000 samples suffice for averaging the error to around 1% of the quantization resolution, so around $0.33 \mu\text{V}$ in the example we consider. We also confirmed that our traces had inter-pulse variations that exceeded 0.7 times the quantization resolution in all traces that we investigated. It is possible that the oscilloscope is designed to satisfy this critical criterion, but it is essential to verify this, and if necessary add variation (e.g., noise), if the quantization error is to be reduced by integration.

Saturation is another possible systematic error. To investigate this, we attenuated the light and investigated the effect on the peak voltage, under representative measurement conditions. We found that the deviations from linearity were around 1 dB in the range from 30 to 300 mV. Linearity was excellent from 3 to 30 mV, and altogether the linearity was found to be within 1 dB ($\sim 20\%$) for 30 dB of dynamic range under representative measurement conditions, if the dark-level is subtracted. Still, this error may seem excessive. However, insofar as the inter-pulse energy is relatively small, it leads to an error in the pulse energy which is much smaller. For example, if the actual inter-pulse energy is 20% of the total energy, the actual ratio of the pulse-to-inter-pulse energy becomes $0.8/0.2$, i.e., 6 dB. A saturation of 1 dB reduces this to 5 dB, i.e., $0.76/0.24$. The error in pulse energy then becomes 5%. It is only in the limit of negligible energy in the pulses that the error in linearity equals the error in pulse energy that results. Although the inter-pulse energy was quite large and even exceeded the pulse energy in some cases, this was for longer pulse durations with lower peak power. For these, deviations from linearity are expected to be smaller and the overall errors were indeed found to be relatively small.

We verified our measurement setup by characterizing seed pulses out from the AOM in Fig. 1 and mixing in controlled amounts of CW light from a separate light source through a fused fiber combiner at the output of the AOM. The resulting pulses were characterized in the same way as those from the FUT, separately for the CW background and the pure pulses (without added background), as well as combined. Attenuators were used to adjust the power levels reaching the detectors to levels similar to those in the experiments with the FUT. The 64-dB extinction ratio of the AOM ensures that the inter-pulse power is negligible at its output. Thus, we were able to synthesize similar pulse traces as obtained from the FUT, but with well-known pulse and inter-pulse energy and the option to eliminate inter-pulse light by switching off the CW source.

Figure 10 shows the integrated voltage for the 6-ns pulse in Fig. 5(a) at 2-kHz PRF as well as for a similar 6-ns “synthetic” case at 1 kHz without and with 0.4 μW of CW background. The average power in the “synthetic” pulses was measured to 10.5 μW . We also checked that the combined power became 10.9 μW . Thus, the inter-pulse energy was 4% of the total. The synthetic trace without added background has an error of $\sim 6 \mu\text{V}$, which results in a decrease in the integrated inter-pulse value of 2.1% of the step (i.e., energy) of that of the pulse. With background, the integrated inter-pulse fraction becomes 6.7%. Although the relative uncertainty in E_{IP} is large, the resulting pulse-energy uncertainty is less than 3% in this case.

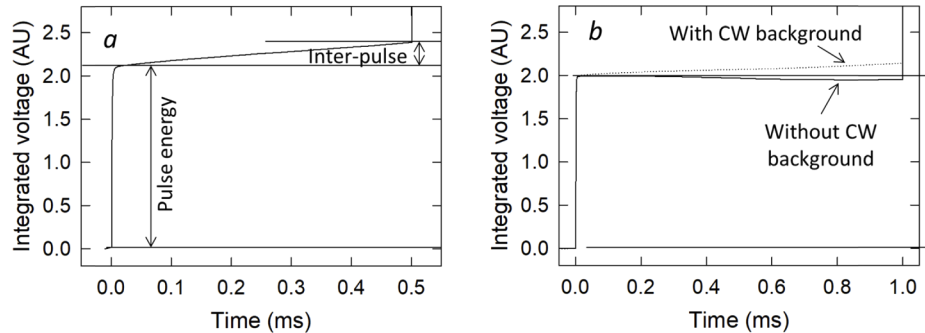


Fig. 10. Integrated oscilloscope trace measured with the slow detector and low-pass filter and with subtracted dark-trace for (a) the pulse in Fig. 5 at 2 kHz and (b) similar “synthetic” pulses at 1 kHz with and without added background.

We also investigated other synthetic pulses to largely cover the range of parameters encountered in the characterization of the FUT. We found that for inter-pulse energies below around 20% according to the integrated trace, the error in pulse energy was below 10%. Although the inter-pulse value was larger than that in some cases, those were for pulses of 200 ns or longer. For such long pulses, the error remained at 10% also for inter-pulse energies of 70%. This may be a result of lower peak power and thus lower detector saturation.

In addition, we simulated the error using a simple detection model with a detector affected by saturation, dark-level error, and a low-pass filter for different pulse parameters. Also according to these simulations, it was possible to reach an error limit of around 10% for our pulse and detection-system parameters. In fact, it was possible to reach this limit for a much wider range of parameters, but this requires that the signal strength is adjusted according to the parameters to a level that seems difficult to know *a priori*. In a similar vein, poorly adjusted measurement parameters such as the power on the detector and the measurement bandwidth can easily lead to large errors. Nevertheless, it seems clear that with appropriate settings, it is possible to determine the pulse energy from most fiber sources of the type we have studied with the approach we have used. We note here that our 226-kHz filter bandwidth seems adequate for the range of 1–40 kHz. 40 kHz is the highest PRF in our data, and might benefit from a larger bandwidth. On the other hand, for low PRFs, a smaller bandwidth may be preferable. Furthermore, a large detector area may be preferable to mitigate saturation, and saturation as well as dark-trace errors can also be reduced by measuring the same pulses with more than one oscilloscope gain setting, and with more than one level of power onto the detector. Although we did not combine data acquired at different settings or light power levels in order to improve the accuracy, we regularly changed these parameters during the experiments to better understand the pulse characteristics and check for anomalies. The traces from which we calculated the pulse energy were generally measured with up to $\sim 0.3\text{-V}$ peak voltage and $\sim 226\text{-kHz}$ filter bandwidth.

To summarize, our measurement accuracy appears to be limited by $\sim 35 \mu\text{V}$ dark-level variations for an oscilloscope setting of 50 mV/division. Deviations from linearity may be significant when

the inter-pulse energy is large. Other identified sources of error are random in nature and become negligible when the signal is integrated (averaged) between pulses. Overall, we estimate errors in reported pulse energies to roughly 10%, perhaps 15% in some cases, but normally less. This does not consider the error in the thermal power meter used for determining average power nor losses in mirrors and lenses. Our investigation has thus shown that with the photodiode and oscilloscope we used, it is generally possible to accurately measure the energy of pulses of around 10 ns or longer at PRF of 1 kHz or more. There are, however, many pitfalls, and care is needed to avoid them.

Funding

University of Southampton (Northrop Grumman Mission Systems); Consejo Tamaulipeco de Ciencia y Tecnología (578927/409382).

Acknowledgments

We acknowledge John Marciante, University of Rochester, for helpful discussions on detector linearity and pulse measurements, Rüdiger Paschotta, RP Photonics, for help with simulations of saturation characteristics in multimode fiber amplifiers Michalis Zervas, University of Southampton, for suggestions on the manuscript.

Disclosures

The authors declare no conflicts of interest.

Data availability

All data supporting this study are available from the University of Southampton at <https://doi.org/10.5258/SOTON/D0853>.

References

1. B. Desthieux, R. I. Laming, and D. N. Payne, "111 kW (0.5 mJ) pulse amplification at 1.5 μm using a gated cascade of three erbium-doped fiber amplifiers," *Appl. Phys. Lett.* **63**(5), 586–588 (1993).
2. V. Philippov, C. Codemard, Y. Jeong, C. Alegria, J. K. Sahu, J. Nilsson, and G. N. Pearson, "High-energy in-fiber pulse amplification for coherent lidar applications," *Opt. Lett.* **29**(22), 2590–2592 (2004).
3. C. Codemard, C. Farrell, P. Dupriez, V. Philippov, J. K. Sahu, and J. Nilsson, "Millijoule, high-peak power, narrow-linewidth, sub-hundred nanosecond pulsed fibre master-oscillator power-amplifier at 1.55 μm ," *C. R. Phys.* **7**(2), 170–176 (2006).
4. S. Desmoulins and F. Di Teodoro, "High-gain Er-doped fiber amplifier generating eye-safe MW peak-power, mJ-energy pulses," *Opt. Express* **16**(4), 2431–2437 (2008).
5. E. Lallier and D. Papillon-Ruggeri, "High energy pulsed eye-safe fiber amplifier," in *CLEO/Europe and EQEC 2011 Conference Digest*, OSA Technical Digest (CD) (Optical Society of America, 2011), paper CJ1_5.
6. E.-L. Lim, S.-U. Alam, and D. J. Richardson, "Optimizing the pumping configuration for the power scaling of in-band pumped erbium doped fiber amplifiers," *Opt. Express* **20**(13), 13886–13895 (2012).
7. G. Canat, W. Renard, E. Lucas, L. Lombard, J. Le Gouët, A. Durécu, P. Bourdon, S. Bordaïs, and Y. Jauouën, "Eyesafe high peak power pulsed fiber lasers limited by fiber nonlinearity," *Opt. Fiber Technol.* **20**(6), 678–687 (2014).
8. I. Pavlov, E. Dülgergil, E. Ilbey, and FÖ İlday, "Diffraction-limited, 10-W, 5-ns, 100-kHz, all-fiber laser at 1.55 μm ," *Opt. Lett.* **39**(9), 2695–2698 (2014).
9. L. Kotov, M. Likhachev, M. Bubnov, O. Medvedkov, D. Lipatov, A. Guryanov, K. Zaytsev, M. Jossent, and S. Février, "Millijoule pulse energy 100-nanosecond Er-doped fiber laser," *Opt. Lett.* **40**(7), 1189–1192 (2015).
10. J. W. Nicholson, A. DeSantolo, M. F. Yan, P. Wisk, B. Mangan, G. Puc, A. W. Yu, and M. A. Stephen, "High energy, 1572.3 nm pulses for CO₂ LIDAR from a polarization-maintaining, very-large- mode-area, Er-doped fiber amplifier," *Opt. Express* **24**(17), 19961–19968 (2016).
11. M. M. Khudyakov, M. M. Bubnov, A. K. Senatorov, D. S. Lipatov, A. N. Guryanov, A. A. Rybaltovsky, O. V. Butov, L. V. Kotov, and M. E. Likhachev, "Cladding-pumped 70-kW-peak-power 2-ns-pulse Er-doped fiber amplifier," *Proc. SPIE* **10512**, 1051216 (2018).
12. G. N. Pearson, P. J. Roberts, J. R. Eacock, and M. Harris, "Analysis of the performance of a coherent pulsed fiber lidar for aerosol backscatter applications," *Appl. Opt.* **41**(30), 6442–6450 (2002).

13. T. A. Driscoll, D. J. Radecki, N. E. Tindal, J. P. Corriveau, and R. Denman, "Self-contained, eye-safe laser radar using an erbium-doped fiber laser," *Proc. SPIE* **4974**, 168–176 (2003).
14. R. Wyatt, "Spectroscopy of rare earth doped fibres," *Proc. SPIE* **1171**, 54 (1990).
15. B. J. Ainslie, "A review of the fabrication and properties of erbium-doped fibres for optical amplifiers," *J. Lightwave Technol.* **9**(2), 220–227 (1991).
16. W. J. Miniscalco, "Erbium-doped glasses for fiber amplifiers at 1500 nm," *J. Lightwave Technol.* **9**(2), 234–250 (1991).
17. Y. Jaouen, G. Canat, S. Grot, and S. Bordais, "Power limitation induced by nonlinear effects in pulsed high-power fiber amplifiers," *C. R. Phys.* **7**(2), 163–169 (2006).
18. S. P. Singh and N. Singh, "Nonlinear effects in optical fibers: origins, management and applications," *Prog. Electromagn. Res.* **73**, 249–275 (2007).
19. E. Snitzer and R. Woodcock, "Yb³⁺-Er³⁺ glass laser," *Appl. Phys. Lett.* **6**(3), 45–46 (1965).
20. V. P. Gapontsev, S. M. Matitsin, A. A. Isineev, and V. B. Kravchenko, "Erbium glass lasers and their applications," *Opt. Laser Technol.* **14**(4), 189–196 (1982).
21. J. E. Townsend, W. L. Barnes, K. P. Jedrzejewski, and S. G. Grubb, "Yb³⁺ sensitised Er³⁺ doped silica optical fibre with ultrahigh transfer efficiency and gain," *Electron. Lett.* **27**(21), 1958–1959 (1991).
22. G. G. Vienne, J. E. Caplen, L. Dong, J. D. Minelly, J. Nilsson, and D. N. Payne, "Fabrication and characterization of Yb³⁺:Er³⁺ phosphosilicate fibers for lasers," *J. Lightwave Technol.* **16**(11), 1990–2001 (1998).
23. D. L. Dexter, "A theory of sensitised luminescence of solids," *J. Chem. Phys.* **21**(5), 836–850 (1953).
24. M. Inokuti and F. Hirayama, "Influence of energy transfer by the exchange mechanism on donor luminescence," *J. Chem. Phys.* **43**(6), 1978–1989 (1965).
25. M. R. Brown, H. Thomas, J. M. Williams, R. J. Woodward, and W. A. Shand, "Experiments on Er³⁺ in SrF₂. III. Coupled-ion effects," *J. Chem. Phys.* **51**(8), 3321–3327 (1969).
26. F. E. Auzel, "Materials and devices using double-pumped phosphors with energy transfer," *Proc. IEEE* **61**(6), 758–786 (1973).
27. J. C. Wright, "Upconversion and excited state energy transfer in rare-earth doped materials," in *Radiationless Processes in Molecules and Condensed Phases (Topics in Applied Physics v. 15)*, F. K. Fong, ed. (Springer-Verlag, 1976), pp. 239–295.
28. V. P. Gapontsev and N. S. Platonov, "Migration-accelerated quenching in glasses activated by rare-earth ions," in *Dynamical processes in disordered systems*, W. M. Yen, ed., (Springer, Aedermannsdorf, Switzerland, 1989).
29. M. Shimizu, M. Yamada, M. Horiguchi, and E. Sugita, "Concentration effect on optical amplification characteristics of Er-doped silica single-mode fibers," *IEEE Photonics Technol. Lett.* **2**(1), 43–45 (1990).
30. P. Blixt, J. Nilsson, T. Carlén, and B. Jaskorzynska, "Concentration dependent up-conversion in Er³⁺-doped fiber amplifiers: experiments and modeling," *IEEE Photonics Technol. Lett.* **3**(11), 996–998 (1991).
31. H. Masuda, A. Takada, and K. Aida, "Modeling the gain degradation of high concentration erbium-doped fiber amplifiers by introducing inhomogeneous up-conversion," *J. Lightwave Technol.* **10**(12), 1789–1799 (1992).
32. E. Delevaque, T. Georges, M. Monerie, P. Lamouler, and J.-F. Bayon, "Modeling of pair-induced quenching in erbium-doped silicate fibers," *IEEE Photonics Technol. Lett.* **5**(1), 73–75 (1993).
33. J. Nilsson, B. Jaskorzynska, and P. Blixt, "Performance reduction and design modification of erbium-doped fiber amplifiers resulting from pair-induced quenching," *IEEE Photonics Technol. Lett.* **5**(12), 1427–1429 (1993).
34. J. L. Wagener, P. F. Wysocki, M. J. F. Digonnet, H. J. Shaw, and D. J. DiGiovanni, "Effect of concentration and clusters in erbium doped fiber amplifiers," *Opt. Lett.* **18**(23), 2014–2016 (1993).
35. M. K. Davis, M. J. F. Digonnet, and R. H. Pantell, "Characterization of clusters in rare earth-doped fibers by transmission measurements," *J. Lightwave Technol.* **13**(2), 120–126 (1995).
36. P. Myslinski, J. Fraser, and J. Chrostowski, "Nanosecond kinetics of upconversion process in EDF and its influence to EDFA performance", Institute for Information Technology, National Research Council, 100/TheE3-1 (1995).
37. E. Maurice, G. Monnom, B. Dussardier, and D. B. Ostrowsky, "Clustering-induced nonsaturable absorption phenomenon in heavily erbium-doped silica fibers," *Opt. Lett.* **20**(24), 2487–2489 (1995).
38. P. Myslinski and J. Chrostowski, "Effects of concentration on the performance of erbium doped fiber amplifier," *J. Lightwave Technol.* **15**(1), 112–120 (1997).
39. B. N. Samson, W. H. Loh, and J. P. de Sandro, "Experimental evidence of differences in the absorption spectra of clustered and isolated ions in erbium-doped fibers," *Opt. Lett.* **22**(23), 1763–1765 (1997).
40. S. Tammela, M. Hotoleanu, K. Janka, P. Kiiveri, M. Rajala, A. Salomaa, H. Valkonen, and P. Stenius, "Potential of nanoparticle technologies for next generation erbium-doped fibers," in *Optical Fiber Communication Conference, Technical Digest (CD)* (Optical Society of America, 2004), paper FB5.
41. D. Boivin, T. Fohn, E. Burov, A. Pastouret, C. Gonnet, O. Cavani, C. Collet, and S. Lempereur, "Quenching investigation on new erbium doped fibers using MCVD nanoparticle doping process," *Proc. SPIE* **7580**, 75802B (2010).
42. A. V. Kir'yanov, Y. O. Barmenkov, G. E. Romero, and L. E. Zarate, "Er³⁺ concentration effects in commercial erbium-doped silica fibers fabricated through the MCVD and DND technologies," *IEEE J. Quantum Electron.* **49**(6), 511–521 (2013).
43. J. Li, Z. Dai, Z. Ou, L. Zhang, Y. Liu, and L. Liu, "Modeling and optimizing of low-repetition-rate high-energy pulse amplification in high-concentration erbium-doped fiber amplifiers," *Opt. Commun.* **282**(17), 3577–3582 (2009).

44. P. G. Rojas Hernández, C. Baker, S. Pidishety, M. Belal, Y. Feng, E. J. Friebele, A. Burdett, D. Rhonehouse, L. B. Shaw, J. Sanghera, and J. Nilsson, "High energy pulse amplification in partly quenched highly Er³⁺-doped fiber," in *Advanced Solid State Lasers 2018*, OSA Technical Digest (online) (Optical Society of America, 2018), paper AM6A.16.
45. L. M. Frantz and J. S. Nodvik, "Theory of pulse propagation in a laser amplifier," *J. Appl. Phys.* **34**(8), 2346–2349 (1963).
46. J. Nilsson and B. Jaskorzynska, "Modeling and optimization of low repetition-rate high-energy pulse amplification in cw-pumped erbium-doped fiber amplifiers," *Opt. Lett.* **18**(24), 2099–2101 (1993).
47. C. C. Renaud, H. L. Offerhaus, J. A. Alvarez-Chavez, J. Nilsson, W. A. Clarkson, P. W. Turner, D. J. Richardson, and A. B. Grudinin, "Characteristics of Q-switched cladding-pumped ytterbium-doped fiber lasers with different high-energy fiber designs," *IEEE J. Quantum Electron.* **37**(2), 199–206 (2001).
48. Q. Fang, Y. Qin, B. Wang, and W. Shi, "11 mJ all-fiber-based actively Q-switched fiber master oscillator power amplifier," *Laser Phys. Lett.* **10**(11), 115103 (2013).
49. B. J. Ainslie, S. P. Craig, S. T. Davey, and B. Wakefield, "The fabrication, assessment and optical properties of high-concentration Nd³⁺ and Er³⁺ doped silica-based fibres," *Mater. Lett.* **6**(5-6), 139–144 (1988).
50. A. Le Sauze, C. Simonneau, A. Pastouret, D. Gicquel, L. Bigot, S. Choblet, A. M. Jurdyc, B. Jacquier, D. Bayart, and L. Gasca, "Nanoparticle Doping Process: towards a better control of erbium incorporation in MCVD fibers for optical amplifiers," in *Optical Amplifiers and Their Applications*, OSA Technical Digest Series (Optical Society of America, 2003), paper WC5.
51. A. Pastouret, C. Gonnet, C. Collet, O. Cavani, E. Burov, C. Chaneac, A. Carton, and J. P. Jolivet, "Nanoparticle doping process for improved fibre amplifiers and lasers," *Proc. SPIE* **7195**, 71951X (2009).
52. I. Savelii, L. Bigot, B. Capoen, C. Gonnet, C. Chaneac, E. Burova, A. Pastouret, H. El-Hamzaoui, and M. Bouzaoui, "Benefit of rare-earth "smart doping" and material nanostructuring for the next generation of Er-doped fibers," *Nanoscale Res. Lett.* **12**(1), 206 (2017).
53. C. Baker, E. J. Friebele, A. A. Burdett, D. L. Rhonehouse, J. Fontana, W. Kim, S. R. Bowman, L. B. Shaw, J. Sanghera, J. Zhang, R. Pattnaik, M. Dubinskii, J. Ballato, C. Kucera, A. Vargas, A. Hemming, N. Simakov, and J. Haub, "Nanoparticle doping for high power fiber lasers at eye-safer wavelengths," *Opt. Express* **25**(12), 13903–13915 (2017).
54. A. I. Burshtein, "Energy transfer kinetics in disordered systems," *J. Lumin.* **34**(4), 167–188 (1985).
55. Y. Feng, B. M. Zhang, J. Zhao, S. Zhu, J. H. V. Price, and J. Nilsson, "Absorption measurement errors in single-mode fibers resulting from re-emission of radiation," *IEEE J. Quantum Electron.* **53**(4), 1–11 (2017).
56. H. Zellmer, A. Tünnermann, H. Welling, and V. Reichel, "Double-clad fiber laser with 30 W output power," in *Optical Amplifiers and Their Applications*, M. Zervas, A. Willner, and S. Sasaki, eds., Vol. 16 of OSA Trends in Optics and Photonics Series (Optical Society of America, 1997), paper FAW18.
57. J. Nilsson, S. Alam, J. A. Alvarez-Chavez, P. W. Turner, W. A. Clarkson, and A. B. Grudinin, "High-power and tunable operation of erbium-ytterbium co-doped cladding-pumped fiber lasers," *IEEE J. Quantum Electron.* **39**(8), 987–994 (2003).
58. A. B. Sripad and D. L. Snyder, "A necessary and sufficient condition for quantization errors to be uniform and white," *IEEE Trans. Acoust., Speech, Signal Process.* **25**(5), 442–448 (1977).
59. P. J. B. Koeck, "Quantization errors in averaged digitized data," *Signal Process.* **81**(2), 345–356 (2001).